ChemComm

ROYAL SOCIETY OF CHEMISTRY

COMMUNICATION

View Article Online
View Journal | View Issue

Cite this: *Chem. Commun.*, 2020, **56**, 3983

Received 30th December 2019,
Accepted 3rd March 2020

DOI: 10.1039/c9cc10055e

rsc.li/chemcomm

Computational and experimental identification of strong synergy of the Fe/ZnO catalyst in promoting acetic acid synthesis from CH_4 and CO_2†

Xiaowa Nie, ‡*[ab] Xianxuan Ren,‡[a] Chunyan Tu,‡[b] Chunshan Song,[ac] Xinwen Guo *[a] and Jingguang G. Chen *[b]

DFT calculations have identified reaction pathways for acetic acid synthesis from CO_2 and CH_4 on ZnO, Cu/ZnO and Fe/ZnO surfaces. Fe/ZnO exhibits strong synergy in facilitating CH_4 activation, dissociation and C–C coupling. Thus, the surface acetate formation is significantly enhanced. The DFT predictions have been confirmed by *in situ* DRIFTS experiments.

Production of valuable chemicals from CO_2 and CH_4 attracts great attention due to their potential utilization as alternative feedstocks while mitigating greenhouse gases, which represents a promising approach in green chemistry and CO_2 utilization.[1] Transformation of CO_2 with CH_4 to value-added products is one of the ideal approaches combining an oxidation and a reduction reaction, however, this process is scientifically and technically challenging, due to the chemical inertness of the two molecules. Acetic acid synthesis is one of the promising reactions in the direct transformation of CO_2 with CH_4 and attracts great interest due to the high market value of acetic acid as an important raw material in the organic chemical industry.[2] This method has 100% atomic efficiency, however, it is thermodynamically unfavorable due to the large positive Gibbs free energy change (ΔG° = 16.98 kcal mol^{-1}). The equilibrium amount of acetic acid formation from the conversion of CO_2 and CH_4 is calculated under different conditions (see Fig. S1, ESI†), which illustrates the dependence on reaction temperature and pressure. Significant efforts have been put into the development of effective catalysts, including homogeneous (*e.g.* $Pd(OAc)_2$/$Cu(OAc)_2$/O_2/CF_3COOH[3]), heterogeneous (*e.g.* metal-exchanged zeolite[4,5]) and photocatalysts,[6] as well as utilizing catalytic dielectric-barrier discharge.[7] Metal oxides and metal-modified zeolites are commonly used as heterogeneous catalysts for the conversion of CO_2 and CH_4.[4,5] However, most of the systems require high temperature to activate and convert both CO_2 and CH_4, and the selectivity and yield of acetic acid are still low (*e.g.* a yield of 395 μmole gcat^{-1} h^{-1} at 773 K[4]). Solid-state NMR spectroscopy has been used to study the mechanism of transformation of CO_2 with CH_4 to acetic acid over Zn-modified HZSM-5 at relatively high temperatures (523 to 773 K).[8] CH_4 activation and dissociation occur at the Zn sites to form a Zn–CH_3* intermediate, the Zn–C bond of which then undergoes the insertion by CO_2 to generate surface acetate species. Acetic acid formation is accomplished by proton transfer from the Brønsted acid site of HZSM-5 to the adsorbed acetate. A recent theoretical study by Zhang *et al.* has reported that the catalytic activity of CO_2 and CH_4 conversion to acetic acid strongly depends on the local structure of active sites of the Zn-modified H-ZSM-5 zeolite.[5] On a Zn-doped ceria catalyst, facile CH_4 activation and C–C coupling are revealed by Ge *et al.* using density functional theory (DFT) calculations.[9] An Eley–Rideal (E–R) mechanism is proposed for surface acetate formation, in which gas phase CO_2 inserts into the σ-bond of Zn–CH_3*. However, the final step of acetic acid formation from acetate hydrogenation is highly endothermic (1.3 eV), limiting the rate of the overall conversion. Their follow-up work has reported concurrent activation of CH_4 and CO_2 at the zinc oxide–indium oxide interface in acetic acid synthesis.[10] The reaction mechanism is altered due to CO_2 adsorption on the defective In_2O_3 surface before insertion into Zn–CH_3*, following a typical Langmuir–Hinshelwood (L–H) mechanism. Although the $(ZnO)_3/In_2O_3(110)$ surface is catalytically more active toward acetic acid formation than $Ga_2O_3/In_2O_3(110)$ and $(ZrO_2)_3/In_2O_3(110)$, both the CH_4 dissociation and CO_2 insertion steps have larger barriers on the mixed oxide surfaces than those obtained over $Zn/CeO_2(111)$ in a previous study.[9]

These studies demonstrate that zinc and zinc oxide are important components for CH_4 activation, however, it is still challenging to simultaneously promote the three key elementary

[a] *State Key Laboratory of Fine Chemicals, PSU-DUT Joint Center for Energy Research, School of Chemical Engineering, Dalian University of Technology, Dalian, Liaoning 116024, P. R. China. E-mail: niexiaowa@dlut.edu.cn, guoxw@dlut.edu.cn*

[b] *Department of Chemical Engineering, Columbia University, New York, NY 10027, USA. E-mail: jgchen@columbia.edu*

[c] *EMS Energy Institute, PSU-DUT Joint Center for Energy Research, Department of Energy & Mineral Engineering, Pennsylvania State University, University Park, PA 16802, USA*

† Electronic supplementary information (ESI) available. See DOI: 10.1039/c9cc10055e

‡ These authors contributed equally to this work.

steps (CH_4 activation, C–C coupling, and H addition) involved in acetic acid formation. The design of active and robust catalysts for acetic acid synthesis directly from CO_2 and CH_4 remains scientifically and practically limited. Fe-based catalysts are active for hydrocarbon and alcohol synthesis *via* promoting C–C coupling and carbon chain growth.[11] Meanwhile, they are also active for CH_4-involved reactions such as conversion to syngas.[12] Therefore, it is of great interest to investigate the role of Fe in the direct transformation of CO_2 with CH_4 to acetic acid, which would be potentially promising when combined with zinc oxide since these two components show good activity in CO_2 or CH_4 related reactions.[10–12] Herein, we present the results of the mechanisms of acetic acid synthesis from CO_2 and CH_4 over the Fe/ZnO catalyst by combining DFT calculations and *in situ* DRIFTS experiments. Parallel studies are conducted on pure ZnO and Cu/ZnO for comparison. For the first time, a strong synergy of the Fe/ZnO catalyst in promoting the acetic acid synthesis from CH_4 and CO_2 is identified, on which the barriers for CH_4 dissociation and C–C coupling are significantly lower than those on ZnO and Cu/ZnO. The side reactions such as CO_2 hydrogenation and CH_3* decomposition can be effectively suppressed on Fe/ZnO, leading to the enhanced production of surface acetate species. The DFT results are confirmed by *in situ* DRIFTS experiments on surface species identification.

On ZnO(10$\bar{1}$0), CH_4 adsorption on the Zn site is weak, with a binding energy of −0.06 eV calculated using the PBE functional and with a dispersion correction of −0.32 eV. CH_4* dissociation occurs through breaking one of the C–H bonds at the Zn site, with the dissociated H atom bonding to an adjacent surface O site (Fig. 1a). The dissociation barrier is 0.93 eV, close to the value (0.97 eV) reported by Shavi *et al.*[13] The CO_2 molecule is adsorbed at the Zn···O–Zn site with a binding energy of −0.83 eV. Subsequent C–C coupling occurs *via* the insertion of CO_2* into the σ-bond of Zn–CH_3*, leading to the formation of a bidentate acetate (η^2-CH_3COO*) species bound to two surface Zn atoms (Fig. S3a, ESI†). The C–C coupling barrier is 1.46 eV and exothermic by 0.73 eV. Therefore, ZnO itself is not active for acetic acid synthesis due to a high C–C coupling barrier and slow CH_4 activation.

When Fe is doped onto the ZnO(10$\bar{1}$0) surface by taking up an O vacancy site, the modified surface electronic properties and structures can induce the alteration of reaction pathways and kinetics, thereby affecting the selectivity and yield of acetic acid. CH_4 adsorption is stronger on the Fe site of Fe/ZnO, with a binding energy of −0.37 eV calculated by PBE and −0.58 eV with dispersion corrections included. The dissociation of CH_4 occurs through breaking one of the C–H bonds at the Fe site, with the dissociated H atom bonding to an adjacent Zn_3 site (Fig. 1b). In the transition state, the H_{diss} atom coordinates to both the Fe and Zn_3 sites, with the H_{diss}–Fe and H_{diss}–Zn_3 distances being 1.70 and 1.84 Å, respectively. The C–H_{diss} bond is lengthened to 1.76 Å, indicating a larger activation degree than the transition state generated on ZnO, which has a C–H_{diss} distance of 1.48 Å. The dissociation barrier is significantly reduced on Fe/ZnO, which is only 0.30 eV, much lower than that (0.93 eV) obtained on pure ZnO. Electronic features are analyzed to explore the observed difference on CH_4 activation/dissociation between ZnO and Fe/ZnO. Bader charge

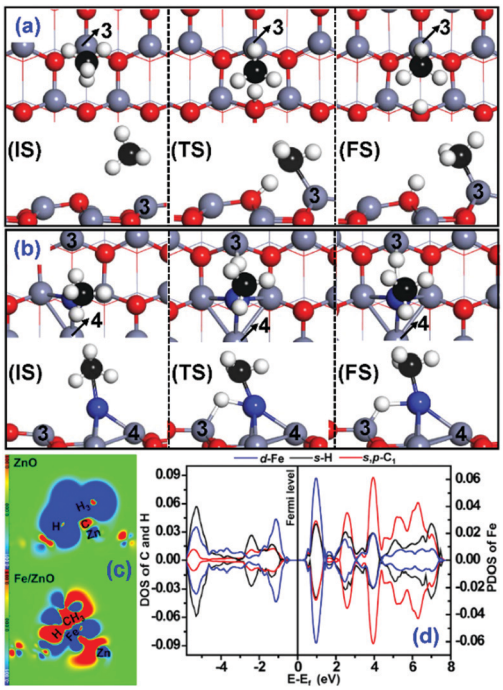

Fig. 1 Optimized structures of the initial, transition and final states associated with CH_4 dissociation on (a) ZnO(10$\bar{1}$0) and (b) Fe/ZnO(10$\bar{1}$0) surfaces (grey: Zn, blue: Fe, red: O, black: C, and white: H). (c) Electron density difference maps of transition states for CH_4 dissociation on the two surfaces. (d) DOS and PDOS of the transition state for CH_4 dissociation on Fe/ZnO(10$\bar{1}$0).

results show that the pure ZnO surface transfers 0.064|*e*| to a CH_4 molecule compared to the transition to the adsorbed state, whereas for Fe/ZnO, Fe metal and ZnO transfer 0.27|*e*| and 0.081|*e*| to CH_4, respectively, rendering CH_4 activation more pronounced in the dissociation process. The electron density difference maps (Fig. 1c) illustrate that on pure ZnO, mainly electron transfer occurs from the ZnO surface to the C atom of CH_3* species but the surface–adsorbate interaction is not strong due to the small electron density accumulation on the CH_3*–H* state. On Fe/ZnO, substantial electron transfer from Fe to CH_3*–H* is observed and the surface–adsorbate interaction is much stronger, making the transition state more stable. These electronic properties are consistent with the trend in the activation barriers, demonstrating an enhanced activity of Fe/ZnO toward CH_4 activation/dissociation. In addition, the density of states (DOS) and projected DOS (PDOS) of the transition state associated with CH_4 dissociation on Fe/ZnO(10$\bar{1}$0) are calculated and shown in Fig. 1d. Significant overlaps between the s and p orbitals of C and d states of Fe are observed, as well as between the s orbital of H_{diss} and d states of Fe. These observations indicate strong interactions between Fe and the CH_3*–H* species, leading to the formation of Fe–C and Fe–H_{diss} bonds in the transition state of CH_4 dissociation.

Subsequent C–C coupling proceeds with Fe–CH_3* and co-adsorbed CO_2 at an adjacent Zn···O–Zn site, following a L–H mechanism for CO_2 insertion (Fig. S3b, ESI†), with a C–C coupling barrier of 0.84 eV. However, the H_{diss} adsorbed at the original dissociated Zn_3···Fe site has a steric effect on C–C coupling.

An alternative pathway is also examined, wherein the H_{diss} first migrates to a $Zn_4\cdots Fe$ bridge site on the other side of Zn_3–CH_3* (Fig. S4, ESI†), which has a barrier of only 0.23 eV. With this new H_{diss} location, the C–C coupling barrier reduces to 0.75 eV. Therefore, both the location and the adsorption stability of H_{diss} have an impact on C–C coupling kinetics over Fe/ZnO. The facile C–C coupling on Fe/ZnO renders it a good candidate for acetic acid synthesis. This C–C coupling barrier is lower than that calculated by Shavi *et al.* on other single oxide catalysts such as CeO_2(111) (2.83 eV)[13] as well as those obtained by Zhao *et al.* on mixed $(ZnO)_3$/In_2O_3(110) (1.45 eV) and Ga_2O_3/In_2O_3 (2.04 eV) surfaces.[10] Electronic features are further analyzed to explain the reduced barrier on Fe/ZnO compared to pure ZnO. The CO_2 molecule acquires 0.749|*e*| and 0.980|*e*| during the formation of C–C coupling transition states on ZnO and Fe/ZnO, respectively, and the transition states on the two surfaces are 0.520|*e*| and 0.717|*e*| negatively charged, respectively. These results are indicative of stronger interactions of CO_2* with both the CH_3* species and the Fe/ZnO surface, enhancing the stability of the transition state. The electron density difference maps (Fig. S3c, ESI†) demonstrate that on Fe/ZnO, substantial electron accumulation is achieved around the C atom of CH_3*, O atom of CO_2* and the H_{diss}, while electrons are depleted around the C atom of CO_2* and surface Fe, indicating strong electronic interactions in CO_2*–CH_3*, Fe–CO_2*, Fe–CH_3* and Fe–H*. Thus, enhanced stability of the transition state for C–C coupling can be achieved on Fe/ZnO, leading to the reduced kinetic barrier. The DOS and PDOS of the C–C coupling transition state (Fig. S3d, ESI†) illustrate substantial overlaps between the s and p orbitals of C_2 in CO_2* and the s and p orbitals of C_1 in CH_3*, showing the tendency of C–C bond formation in the transition state. Overlaps between the d states of Fe and the s and p orbitals of C_1 in CH_3* indicate that the binding interaction of Fe–CH_3* still plays a role in transition state formation, consistent with the transition state configuration shown in Fig. S3b (ESI†). CO_2* interacts with both the Zn_1 and Fe sites and orbital overlaps of the s orbital of Zn with the s and p orbitals of O_1 in CO_2* and the d states of Fe with the s and p orbitals of C_2 in CO_2* are observed. These results demonstrate strong bimetallic synergy of Fe–Zn in promoting C–C coupling between Fe–CH_3* and CO_2*.

The C–C coupling leads to the formation of an adsorbed bidentate acetate (η^2-CH_3COO*) species. On pure ZnO, η^2-CH_3COO* is bound to the surface Zn_1 and Zn_3 sites and the direct hydrogenation of O_2 with H_{diss} produces an acetic acid product. This H addition step has a small barrier of 0.32 eV with the reaction being endothermic by 0.27 eV. Acetic acid desorption should be kinetically slow, with a desorption energy of 1.09 eV. On Fe/ZnO, the η^2-CH_3COO* species binds to the Zn_1 and Fe sites. CH_3COO* hydrogenation with the H_{diss} adsorbed at the $Zn_4\cdots Fe$ bridge site needs to overcome a large barrier (1.95 eV) and a strong endothermic reaction energy (1.85 eV). Instead, another H_{diss} migration step is explored before acetic acid formation on Fe/ZnO, in which the H_{diss} migrates to a surface O_3 site prior to acetate hydrogenation (Fig. S4, ESI†). Although the migration barrier (0.99 eV) is not small, it is more favorable than the direct hydrogenation of acetate. More importantly, with this new H_{diss} location, the acetic acid formation becomes more facile, with a reaction energy of only 0.2 eV and zero barrier. It is worth noting that the produced CH_3COOH* is in a metastable state on both ZnO and Fe/ZnO, in which the H_{diss} atom also strongly interacts with the surface O_3 site while binding to O_1 of CH_3COOH* (Fig. S5, ESI†). Although the final desorption of acetic acid from the surface is slow, formation of the surface acetate species is dramatically more favorable on the Fe/ZnO surface, due to the fast CH_4 activation/dissociation, facile C–C coupling, and easy H addition.

In the synthesis of acetic acid using heterogeneous catalysts, several by-products such as formic acid and methanol are detected in experiments.[2] Here, the formation of the primary by-product formic acid (HCOOH) is examined over Fe/ZnO($10\bar{1}0$), which can be produced from CO_2* hydrogenation *via* a COOH* or HCOO* intermediate (Fig. S6, ESI†). The barriers are 1.64 and 1.43 eV for COOH* and HCOO* formation, respectively, indicating that the production of the formic acid by-product is not facile on Fe/ZnO. In addition, the dissociation of CH_3* to CH_2* + H* has a barrier of 1.19 eV, kinetically unfavorable compared to the C–C coupling of CH_3* with CO_2* (0.75 eV). These DFT results reveal that the side reactions are significantly suppressed on Fe/ZnO (Fig. S7, ESI†), leading to an enhanced selectivity to the desired acetic acid product.

To shed light on whether other 3d transition metal doped ZnO has comparable activity to Fe/ZnO, similar calculations are performed on Cu/ZnO. The DFT results are provided in the ESI.† The pathways for acetic acid formation on Cu/ZnO are similar to those on Fe/ZnO, but its catalytic activity should be much lower than that of Fe/ZnO, as illustrated in Fig. 2. In particular, CH_4 dissociation and C–C coupling have larger barriers on Cu/ZnO, making the formation of surface acetate species more difficult. However, formate formation from CO_2 hydrogenation is facile, with a barrier of 1.12 eV. Therefore, formate would be the dominant surface species during the CO_2 reaction with CH_4 on Cu/ZnO.

In situ DRIFTS experiments have been conducted to identify the surface species formation during the CH_4 + CO_2 reaction and after purging reactants over ZnO, Cu/ZnO and Fe/ZnO (Fig. 3). Two strong bands at 1500–1520 cm^{-1} and 1320–1340 cm^{-1} are assigned to monodentate carbonates.[14,15] Under reaction conditions, only monodentate carbonates (1508 and 1332 cm^{-1}) and some hydrogen carbonates (1607 and 1375 cm^{-1})[15] are formed on the surface of a ZnO support, indicating that ZnO itself is not active for converting CO_2 + CH_4. The monodentate carbonates are also observed on Cu/ZnO and Fe/ZnO, which originated from CO_2 adsorption over the O sites. Typical stretching vibrational modes of formate at 1592 and 1369 cm^{-1} are observed on Cu/ZnO and Fe/ZnO.[15,16] However, Cu/ZnO exhibits stronger features of formate species, indicating that formate is the dominant surface species during the conversion of CO_2 and CH_4 (consistent with the DFT results). When removing the reactants of CO_2 and CH_4 from the DRIFTS cell, the vibrational modes of formate species become weaker gradually and diminish after 30 min. Interestingly, unlike ZnO and Cu/ZnO, the Fe/ZnO catalyst shows the O–C=O stretching modes at 1538 and 1448 cm^{-1} under the reaction conditions of the CO_2 + CH_4 mixture, which are assigned to the surface bidentate acetates (η^2-CH_3COO*).[16,17] These species completely disappear after purging the reactants for 10 min, suggesting that the bidentate acetate formed on Fe/ZnO is an active surface intermediate. In order to further identify the formation of

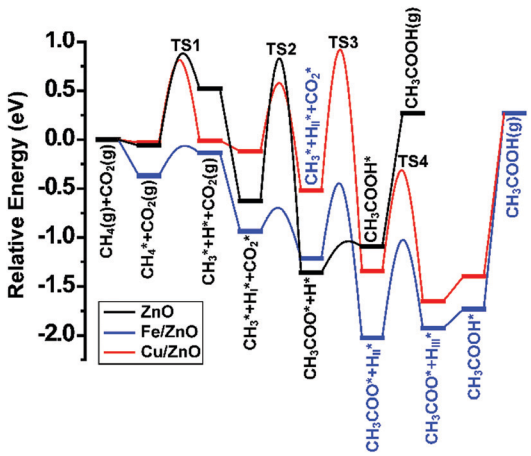

Fig. 2 Energy profiles of acetic acid synthesis from CO_2 and CH_4 on ZnO($10\bar{1}0$), Cu/ZnO($10\bar{1}0$) and Fe/ZnO($10\bar{1}0$) surfaces (H_I* denotes the initial H_{diss} site from CH_4 dissociation, H_{II}* represents the first H_{diss} migration from the initial $Zn_3\cdots M$ to $Zn_4\cdots M$ bridge site, and H_{III}* stands for the second H_{diss} migration from the $Zn_4\cdots M$ bridge site to the surface O_3 site on Cu/ZnO and Fe/ZnO).

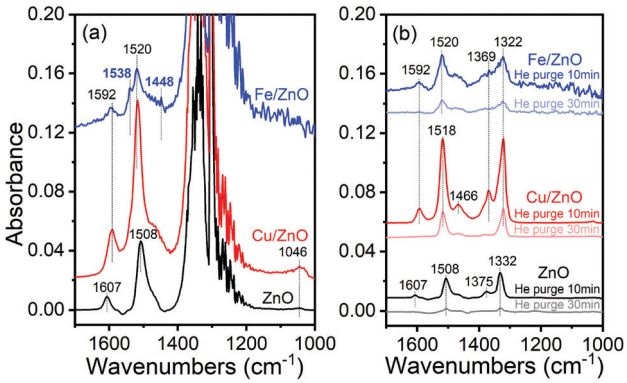

Fig. 3 *In situ* DRIFTS spectra of (a) the CH_4 + CO_2 reaction and (b) spectra after He purge over ZnO, Cu/ZnO and Fe/ZnO at 673 K.

surface bidentate acetate on Fe/ZnO, a "CH_4 off–CH_4 on" experiment is performed to observe the dynamic changes of surface species over Fe/ZnO (Fig. S12, ESI†). No bands at around 1538 and 1448 cm^{-1} are observed during the adsorption of CO_2 alone for 30 min. However, when CH_4 is introduced into the CO_2 gas stream, peaks at 1538 and 1448 cm^{-1} appear and become more intense after 30 min. These two new bands are attributed to surface bidentate acetate formed on Fe/ZnO, which are identical to those species formed by the adsorption of acetic acid.[16,17] These peaks become invisible gradually after cutting off CH_4 and CO_2, confirming that active surface acetate species are formed in the presence of both CH_4 and CO_2 on Fe/ZnO under the reaction conditions. The detection of monodentate carbonates on ZnO, Cu/ZnO and Fe/ZnO identified by DRIFTS is also consistent with DFT calculations (see Fig. S3 and S8, ESI†). Therefore, the DFT-predicted synergy of Fe/ZnO in facilitating acetate formation is supported by the *in situ* DRIFTS experiments.

In conclusion, DFT calculations reveal reaction pathways for acetic acid synthesis from CO_2 and CH_4 on ZnO, Cu/ZnO and Fe/ZnO surfaces. ZnO itself is not active due to large barriers for CH_4 activation and C–C coupling. Cu/ZnO is catalytically inactive either, due to large barriers for CH_4 dissociation, C–C coupling and surface H* migration, while formate is the dominant surface species in the conversion of CO_2 and CH_4 on this surface. Doping ZnO with Fe leads to a strong synergy in promoting acetic acid formation, with both CH_4 activation/dissociation and C–C coupling being facilitated. Consequently, the formation of surface acetate species is significantly enhanced. The DFT results on comparing the pathways and activities of the three catalysts are verified by the *in situ* DRIFTS experiments. This work provides insights into the understanding of mechanisms for acetic acid synthesis from CO_2 and CH_4 and paves a way for designing efficient transition metal doped ZnO catalysts for future studies.

This work is supported by the National Key Research and Development Program of China under Contract No. 2016YFB0600902. C. T. and J. G. C. acknowledge support by the U.S. Department of Energy (DOE), Catalysis Science Program, under Contract No. DE-SC0012704. We acknowledge Dr Zhenhua Xie for performing calculations of thermodynamic equilibrium concentrations.

Conflicts of interest

There are no conflicts to declare.

References

1 C. Song, *Catal. Today*, 2006, **115**, 2–32.
2 W. Huang, K. C. Xie, J. P. Wang, Z. H. Gao, L. H. Yin and Q. M. Zhu, *J. Catal.*, 2001, **201**, 100–104.
3 K. Masanobu, N. Kazuyuki, J. Tetsuro, T. Yuki, T. Ken and F. Yuzo, *Chem. Lett.*, 1995, **24**, 244.
4 A. M. Rabie, M. A. Betiha and S.-E. Park, *Appl. Catal., B*, 2017, **215**, 50–59.
5 P. Zhang, X. Yang, X. Hou, J. Mi, Z. Yuan, J. Huang and C. Stampfl, *Catal. Sci. Technol.*, 2019, **9**, 6297–6307.
6 N. Yazdanpour and S. Sharifnia, *Sol. Energy Mater. Sol. Cells*, 2013, **118**, 1–8.
7 C. J. Liu, L. Yang, Y. P. Zhang, Y. Wang, J. J. Zou, E. Baldur and B. Z. Xue, *Chem. Lett.*, 2001, **30**, 1304–1305.
8 J.-F. Wu, S.-M. Yu, W. D. Wang, Y.-X. Fan, S. Bai, C.-W. Zhang, Q. Gao, J. Huang and W. Wang, *J. Am. Chem. Soc.*, 2013, **135**, 13567–13573.
9 Y. Zhao, C. Cui, J. Han, H. Wang, X. Zhu and Q. Ge, *J. Am. Chem. Soc.*, 2016, **138**, 10191–10198.
10 Y. Zhao, H. Wang, J. Han, X. Zhu, D. Mei and Q. Ge, *ACS Catal.*, 2019, **9**, 3187–3197.
11 H. Yang, C. Zhang, P. Gao, H. Wang, X. Li, L. Zhong, W. Wei and Y. Sun, *Catal. Sci. Technol.*, 2017, **7**, 4580–4598.
12 N. Deshpande, A. Majumder, L. Qin and L. S. Fan, *Energy Fuels*, 2015, **29**, 1469–1478.
13 R. Shavi, J. Ko, A. Cho, J. W. Han and J. G. Seo, *Appl. Catal., B*, 2018, **229**, 237–248.
14 A. M. Turek, I. E. Wachs and E. DeCanio, *J. Phys. Chem.*, 1992, **96**, 5000–5007.
15 G. N. Vayssilov, M. Mihaylov, P. S. Petkov, K. I. Hadjiivanov and K. M. Neyman, *J. Phys. Chem. C*, 2011, **115**, 23435–23454.
16 V. Matsouka, M. Konsolakis, R. M. Lambert and I. V. Yentekakis, *Appl. Catal., B*, 2008, **84**, 715–722.
17 W. Rachmady and M. A. Vannice, *J. Catal.*, 2002, **207**, 317–330.

